Multitemporal monitoring of Impervious Surface Areas (ISA) changes in an Arctic setting, using ML, Remote Sensing data and GEE

Authors: *Katerina Dermosinoglou[1], Spyridon E. Detsikas[1], George P. Petropoulos[1], Loukia-Maria Fratsea[1], Apostolos G. Papadopoulos[1]*

[1]Department of Geography, Harokopio University of Athens, El. Venizelou 70, Kallithea, Athens, 17671, Greece

Abstract

The impact of climate change in Arctic regions, due to the character of its ecosystem, the wealth of natural resources and the increased development of activities, is becoming more and more significant and leads to a further increase of environmental problems. The particular characteristics of these regions, including harsh climatic conditions and limited infrastructure, render essential the use of specific approaches to monitor and plan urban growth.

The main objective of this study is the multi-temporal mapping of urban changes, through Impervious Surface Areas (ISA), over the past decade in an Arctic settlement under high structural density. This endeavor is implemented through the use of Machine Learning classification methods, applied on the pixel level in a time series of Landsat imagery data, were tested while the execution of the required processing was carried out in Google Earth Engine (GEE) cloud platform.

The results of this study detect with high accuracy ISA changes in Tromso area from 1993 to 2023. The insights gained from this study have the potential to enhance our knowledge about the dynamics behind urban expansion, the main elements associated with urban sprawl and their interaction with climate change challenges in permafrost environments.

Keywords: *EO-PERSIST, ISA, Google Earth Engine, Remote Sensing, Arctic*

1. INTRODUCTION

The term of Impervious Surface Areas (ISA) is used to describe man-made land surface features, acting like barriers, preventing water infiltration into soil. This term includes structures like buildings, paved roads, driveways, sidewalks, parking lots, and rooftops (Weng, 2007; Popa et al., 2023) while holds a critical source of understanding the environmental, ecological, and hydrological aspects of urban planning. Over the past five decades, there has been a rapid global expansion of the ISA, reaching approximately 0.62 million km^2 from 1972 to 2019 (Huang et al., 2021), trend closely linked to the United Nations' report (2018) on urbanization trends which reveals that 55% of the world's population, more than half, resided in urban areas in 2017 and this percentage is expected to increase to 68% by 2050. At the same time, human activities including energy exploitation and urban development, have significantly contributed to ISA expansion in the Arctic region (Lifshits et al., 2021; Nguyen et al., 2021; Usman et al., 2022). These trends highlight the strong correlation between ISA and human influence while offer a focal point for further studies that thoroughly explore the interaction of these two factors.

Recognizing the critical role of ISA, there is a need for consistent monitoring and mapping of those areas. A large number of ISA mapping research has been addressed using Earth Observation (EO), which provides remarkable benefits in monitoring ISA, as it offers time and cost-efficient images that can be used to map globally the ISA expansion. Landsat archive has been a cornerstone EO mission

in ISA mapping, as it is the most extensive and consistent medium resolution EO data source (Chaudhuri et al., 2017; Schug et al., 2018; Cao et al., 2020; Xu et al., 2022). Apart Landsat, various studies have used Sentinel imagery, including both the optical instrument Sentinel-2 (Feng and Fan, 2021; Kumar et al., 2020) and Synthetic Aperture Radar (SAR) images from Sentinel-1 (Shrestha et al., 2021; Wu et al., 2023). Additionally, many studies have extracted ISA from various SAR images, including ALOS/PALSAR images (Attarchi, 2020), TerraSAR-X images (Zhang et al., 2016), and ENVISAT Advanced Synthetic Aperture Radar (Zhang et al., 2014) while also, a significant amount of research has been directed at identifying and mapping ISAs through high-resolution images, such as IKONOS (Lu and Weng, 2008; Olufayo Adetoro, 2022), WorldView (Olufayo Adetoro, 2022), SPOT-5 (Xu, 2013), and GF-2 (Wang et al., 2022). It is worth noting that, only a limited number of studies have explored the application of hyperspectral images in ISA extraction, applying data such as Hyperion (Tang and Xu, 2017; Liu and Gu, 2017), GF-5 (Liu et al., 2020), or EnMAP imagery (Feng and Wang, 2018). Given the abundance of the existing EO datasets, the processing challenges have increased. Those challenges are addressed by using cloud-based platforms like Google Earth Engine (GEE) which offer a cost-effective and computationally efficient means to process large-scale EO data. Despite the rapid growth in the use of such cloud platforms, their applicability for ISA mapping seems to be limited, as suggested by the number of relevant studies in the published literature.

For the mapping of ISA, different techniques of image processing are leveraged, all originating from EO datasets. These techniques can be generally grouped into three categories: index techniques, methods of classification, and spectral mixture analysis (SMA) (Feng et al., 2019; Pandey e-t al., 2019). Index methods, which involve creating an index based on spectral differences between impervious surfaces and other land features, have gain attention for their computational straightforwardness. Zha et al. (2003) devised the Normalized Difference Built-up Index (NDBI) by exploiting near-infrared and shortwave-infrared bands. In a similar vein, Xu (2008) introduced the Index-based Built-up Index (IBI), by merging NDBI, Soil Adjusted Vegetation Index (SAVI), and the modified Normalized Difference Water Index (mNDWI) while Xu (2010) also formulated the Normalized Difference Impervious Surface Index (NDISI) based on mNDWI, near-infrared, and shortwave-infrared bands. The Combinational Built-up Index (CBI) was innovated by combining NDWI, SAVI, and PC1, the first principal component (Sun et al., 2016), while the Normalized Difference Impervious Index (NDII) was established by combining the visible and thermal bands (Wang et al., 2015). Fang et al. (2019) introduced the Ratio-based Impervious Surface Index (RISI), a novel index for extracting ISA from Landsat imagery, incorporating the coastal band (B1) and the Normalized Difference Vegetation Index (NDVI). Tian et al. (2018) developed the Perpendicular Impervious Surface Index (PISI) using the blue and near-infrared bands of Landsat 8 data for mapping ISAs.

In terms of classification methods, separating pixels into impervious and non-impervious categories, based on their spectral signatures, is a widely used (Fang et al., 2019). Support Vector Machine (SVM) stands out as one of the most frequently employed methods for ISA extraction, with studies confirming its effectiveness (Feng et al., 2021). Shi et al. (2017) utilized SVM to map ISAs from 1987 to 2016 using Landsat time series, yielding accurate results while also other studies demonstrated the efficiency of SVM classifier in ISA mapping (Cheng et al., 2011; Elatawneh et al., 2012; Petropoulos et al., 2012a; Petropoulos et al., 2012b; Okujeni et al., 2013; Whyte et al., 2018; Cass et al., 2019; Mugiraneza et al., 2020; Fragou et al., 2020;). Additionally, Random Forest (RF) is characterized as a convenient method (Shrestha, 2021; Liu et al., 2020), and Kumar et al. (2020) compared SVM, RF, and Neural Network (NN) classification techniques, identifying NNs as the most accurate for extracting built-up ISAs using high-resolution satellite data. Huang et al. (2018) demonstrated the effective application of deep learning methods for ISA extraction, leveraging high-resolution

WorldView and Pleiades images. In particular, various studies have applied deep learning methods to map ISAs using moderate-resolution images such as Landsat (Dawson et al., 2019; Parekh et al., 2021; Xu et al., 2022). The Object-Based Image Analysis (OBIA) approach has also found wide application in ISA extraction, especially with high-resolution images (Hu and Weng, 2011; Petropoulos et al., 2012c; Sebari and He, 2013; Zhang et al., 2013).

The present research targets to map ISA in the Tromso region while also analyze the transitions in these surfaces over the past three decades. Additionally, it seeks to verify any potential correlation between these changes and local population fluctuations since the year 1990.

2. DATA AND METHODOLOGY

2.1. STUDY AREA

Situated north of the Arctic Circle, the island-city of Tromso is the most populated city in northern Norway (De Melo Cartaxo et al., 2021). With a thriving population of 77.544 (Statistics Norway, 2022), this affluent Arctic capital is linked to the mainland by the Tromso Bridge and Tromsoysund Tunnel, while also being connected to Kvaloya Island via the Sandnessund Bridge. Tromso, belonging to Troms County, holds historical significance as a vital economic force in Norway, dating back centuries. Before obtaining city status in 1794, it served as the gateway to the Arctic, functioning as a crucial meeting and starting point for renowned Arctic explorations. The Norwegian Sea, enveloping the city and stretching beyond its limits, constitutes a marginal sea within the Arctic Ocean, teeming with abundant resources. Presently, the Norwegian Sea maintains its importance as a key avenue for transport and communication. Through its natural resources, it continues to foster profitable industries, contributing to a thriving local economy.

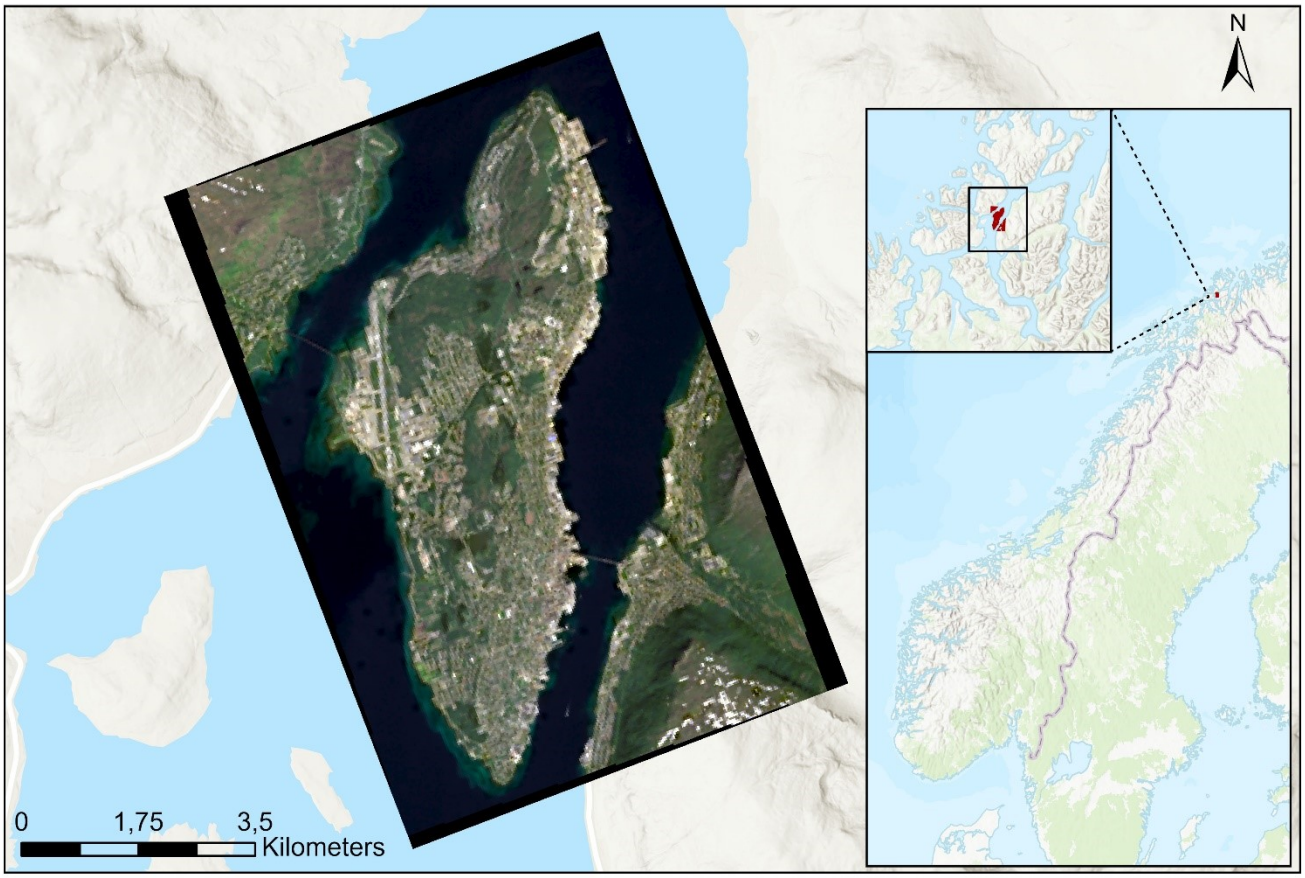

Figure 2.1. Study area map (Landsat 9 image, 20/06/2023)

Tromso's subarctic climate is marked by substantial snowfall and chilly winds throughout its extended winters, which endure for approximately six months. Polar nights, extending from late November to mid-January, contribute to prolonged darkness. Additionally, precipitation in the form of rain is not uncommon, frequently resulting in the formation of icy and slippery road surfaces, thereby posing hazardous driving conditions. Tromso's subarctic climate is marked by substantial snowfall and cold winds throughout its extended winters, which endure for approximately six months. Polar nights, extending from late November to mid-January, contribute to prolonged darkness. Additionally, precipitation in the form of rain is not uncommon, frequently resulting in the formation of icy and slippery road surfaces, thereby posing hazardous driving conditions.

2.2. DATASET DESCRIPTION

The present research utilizes Landsat imagery to conduct multitemporal monitoring of ISA in Tromso. Landsat, characterized by its moderate spatial resolution, offers extensive coverage of data over large areas. Specifically, Landsat 5 Thematic Mapper (TM) and Landsat 9 Operated Land Imager (OLI), Collection 2 Surface reflectance products were employed in this study. All the selected for this study images (Table 2.1), were acquired on anniversary dates, during summer months, to minimize the presence of significant cloud cover and ensure that the identified changes are not caused by any natural or other factor.

Table 2.1. Landsat images acquired in the study

Date	Satellite	Dataset
23/08/1993	Landsat 5	*LANDSAT/LT05/C02/T1_L2/LT05_199011_19930829*
13/08/2007	Landsat 5	*LANDSAT/LT05/C02/T1_L2/LT05_198011_20070813*
30/06/2023	Landsat 9	*LANDSAT/LC09/C02/T1_L2/LC09_198011_20230630*

Three specific dates were chosen, starting from 1993 and ending in 2023. The original intention was to acquire the third image precisely at the midpoint of this period, specifically during the summer of 2008. However, due to the lack of Landsat data with a cloud coverage percentage conducive to image processing, an image from the corresponding months of 2007 was chosen instead.

Furthermore, to be created a correlation pattern between changes in ISAs and alterations in social factors, demographic data for the broader Tromso region were utilized, sourced from the Statistical Service of Norway. Specifically, population data from 1990 to 2022 were obtained.

2.3. METHODOLOGY DESCRIPTION

The SVM method is used in this study to detect changes in ISA from 1993 to 2023. The entire following process has been implemented in Google Earth Engine (GEE) cloud platform, as shown in Figure 2.2.

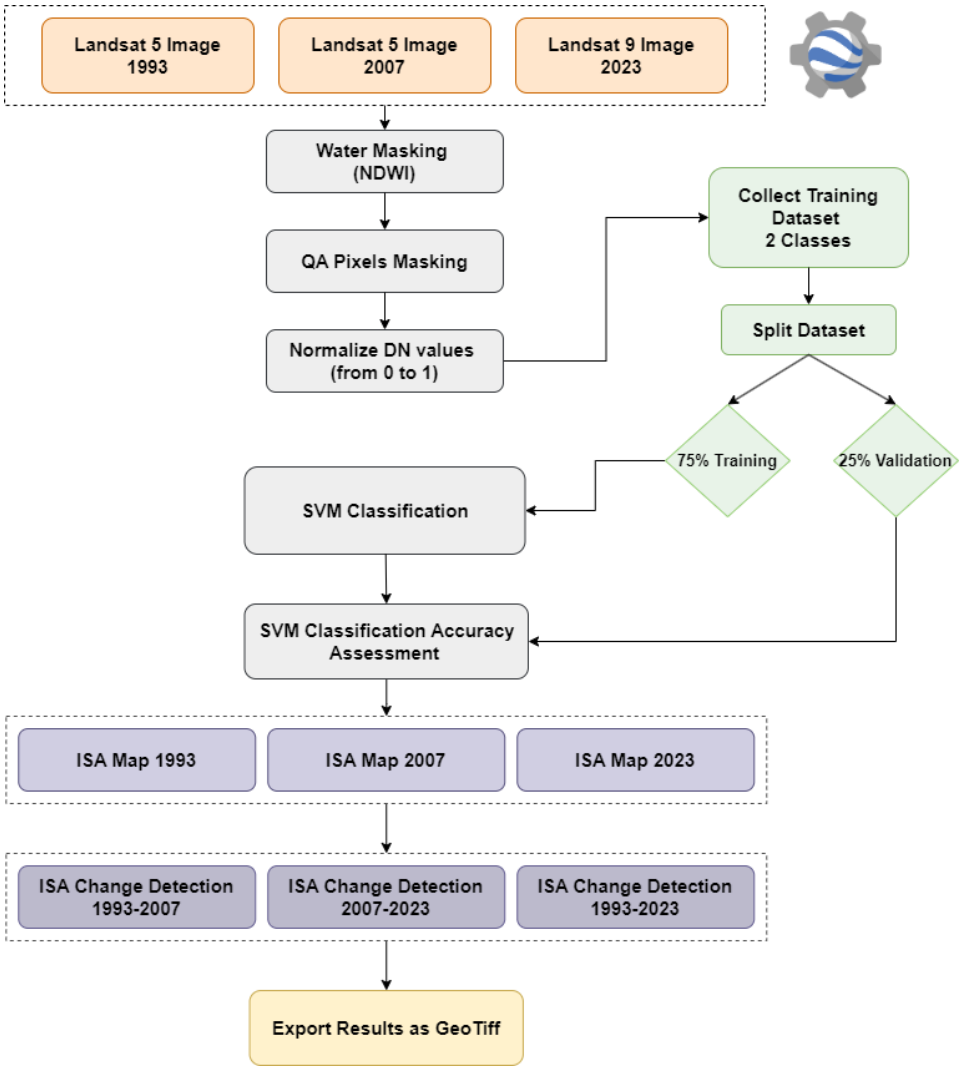

Figure 2.2. Methodology flowchart

2.3.1. DATA PRE-PROCESSING

Landsat images were selected directly from GEE platform, according to their cloud cover percentage (less than 30%). Due to the geographical characteristics of the study area, acquiring images with cloud cover below 10% posed a considerable challenge. As the images obtained were already geometrically and atmospherically corrected, no additional processing was required. The first step was to bound the study area, using a polygon and apply the Normalized Difference Water Index (NDWI) to mask out all water bodies. The subsequent step involved QA pixel masking to eliminate clouds, cloud shadows, and unused pixels from the images. The final step of the pre-processing procedure entailed applying a scale factor of 0.0000275 and the offset of -0.2 standardizing all values on a conceptual scale ranging from 0 to 1.

2.3.2. CLASSIFICATION AND CHANGE DETECTION

Along the lines of other studies like Huang et al. (2021) and Liu et al. (2023), it is also implemented herein binary classification which included the classes of Impervious and Non-Impervious, as the primary goal was to exclusively extract ISA. Before applying SVM classifier to the three images, the first step was the generation of train – validation datasets. Three different datasets were created, each corresponding to a specific date, by stratified sampling, mainly based on the false – color composite (NIR, RED, GREEN bands) which better points out the ISA (Li et al., 2013) and SWIR bands. The dataset's points number follows the rule of 10N to100N, where N is the number of bands used for the analysis. For both Landsat 5 images (6 bands) and Landsat 9 images (7 bands), almost 350 points were carefully selected, per class. Subsequently, the datasets were split into training and validation samples. 75% of the total points were allocated for training the classifier, with the remaining 25% used for validation. The SVM machine learning classifier was trained and performed for all dates by default parameters.

The final phase of the entire process involved implementing Change Detection (CD) in GEE platform and calculating the areas undergoing change. Post classification comparison has been employed as the most effective change detection method as the data were individually classified and normalized. This approach diminishes disparities between the dates, rendering it a robust method (Sun et al., 2009; Vivekananda et al., 2021). The ISA alterations were mapped chronologically, into pairs (i) from 1993 to 2007, (ii) from 2007 to 2023 and (iii) from 1993 to 2023. For all these dates, only changes from Non-ISA to ISA were calculated, the changed area was quantified in km^2, based on the pixel size, and was turned into percentage of change, relative to the total size of the study area. The layers were visualized using the ArcGIS Pro software, and the outcomes are presented in Section 3.

2.3.3. VALIDATION APROACH

The evaluation of ISA was conducted through a comprehensive analysis of various statistical indices (Congalton, 1991), including Cohen's Kappa (Kc), overall accuracy (OA), user's accuracy (UA) and producer's accuracy (PA). Kappa serves as a measure of agreement between the reference data and the classification, relative to the probability of agreement between the reference data and a random classifier. Overall accuracy quantifies the likelihood of a pixel being accurately classified by the thematic map. The user's accuracy identifies pixels that, though not genuinely belonging to a reference class, are incorrectly assigned to other ground truth classes while producer's accuracy carefully examines the pixels omitted from their reference class. Kappa (Kc) is a dimensionless metric ranging from 0 to 1, while the remaining statistical metrics are expressed as percentages (%). The values of OA, PA, UA as well as kappa coefficient were also automatically calculated in GEE platform, by using the validation samples that were created.

3. RESULTS

The results of the SVM classifier are shown in Figures 3.1, 3.2, 3.3, while the comprehensive summary of the statistical results concerning the accuracy assessment of the classification is included in Table 3.1. It should be noted that the term "null" pertains to pixels that have been excluded from the QA masking. The outcomes of the multi-temporal classification reveal a continuous expansion of ISAs over the investigated chronological span. To elaborate, a marginal variation in ISA is discerned from 1993 to 2007, registering at approximately 0.22%. In contrast, a highly accelerated change is observed during the temporal interval spanning 2007 to 2023, reaching 4%.

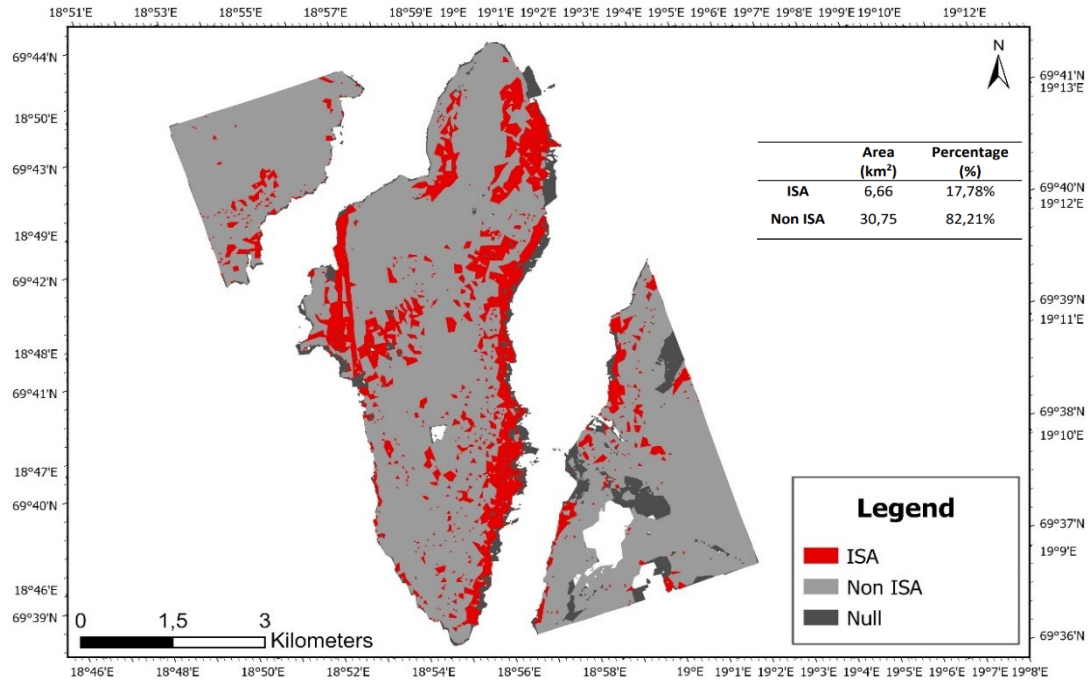

Figure 3.1. Classification results of the Tromso Area using the SVM classifier, 1993. (Pixels removed from QA masking are represented as "Null")

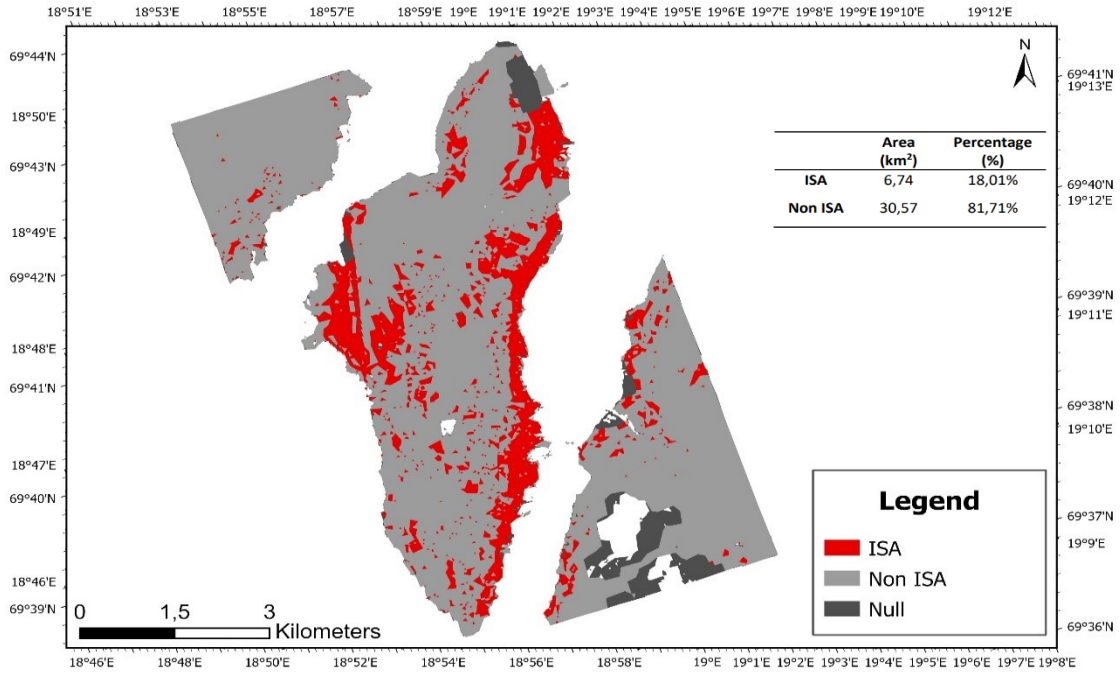

Figure 3.2.. Classification results of the Tromso Area using the SVM classifier, 2007. (Pixels removed from QA masking are represented as "Null")

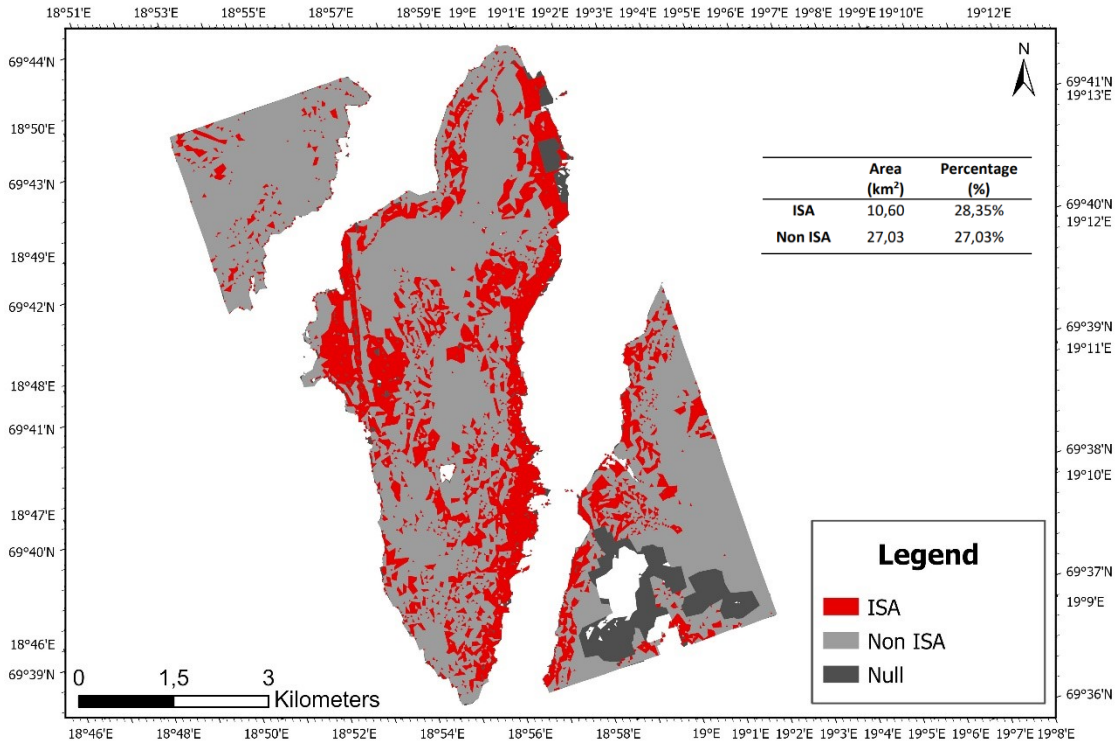

Figure 3.3.. Classification results of the Tromso Area using the SVM classifier, 2023. (Pixels removed from QA masking are represented as "Null")

In 1993, ISAs covered an area of 6,66 km^2 or 17,79% of the total area, spanning nearly the entire territory of Tromso Island. The primary settlement of Tromso in the east, as well as the airport in the western part of the island, are easily discernible. In 2007, ISA occupied an area of 6.74 km^2, constituting 18.01% of the total area. The urban fabric of Tromso appears more contiguous, with an observable increase in ISA around the airport area. Pixels that have been removed in the northern part of the island can be assumed to have been ISA, both from the 1993 classification results and from surrounding pixels. Finally, in 2023, a substantial expansion of ISA is observed, covering 10.6 km^2, accounting for approximately 30% of the total area. In this scene, ISA is also identified in the eastern part of the study area, delineating the growth of the Tromsdalen settlement. This quantitative alteration of ISA is presented in Figure 3.7.

The accuracy assessment for all classifications was conducted using the confusion (error) matrix, which is presented in Table 3.1. It is obvious that the methodology used in the present study leads to highly accurate results, according to the following metrics. The OA reached 93,18%, 95,13% and 90,19% for 1993, 2007 and 2023 respectively, while kappa coefficient was 0,864, 0,903 and 0,802. As for the rest of the accuracy metrics, PA took values from 91,2% to 95,71%, percentages that strongly

indicate a high probability that the classification of each class aligns closely with reality. UA values ranged from 88,63% to 95,74% providing the accurate and subjective selection of training samples.

Table 3.1. Confusion matrix results

	1993		2007		2023	
	PA(%)	**UA(%)**	**PA(%)**	**UA(%)**	**PA(%)**	**UA(%)**
ISA	95,29	91,01	95,55	94,50	93,97	88,63
Non ISA	91,20	95,40	94,73	95,74	95,71	92,30
OA	93,18		95,13%		90,19%	
kappa	0,864		0,903		0,801	

Based on the classification, results presented above, a CD analysis was performed in order to map the ISA changes. The change detection analysis was processed in three series (a) 1993 to 2023; (b) 1993 to 2007; (c) 2007 to 2023 and were selected only changes from non-Impervious to Impervious class. In Figures 3.4, 3.5 and 3.6, are demonstrated the results of this analysis based on SVM classification.

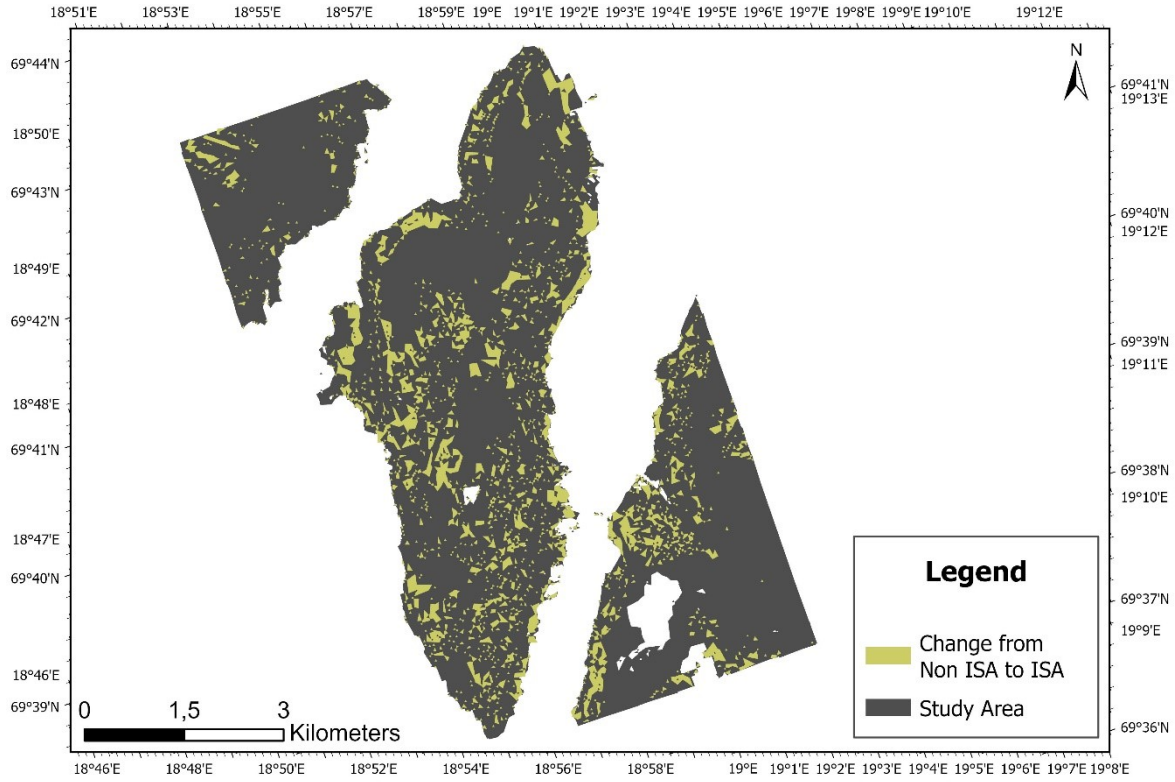

Figure 3.4. Change detection results for 1993-2023 period

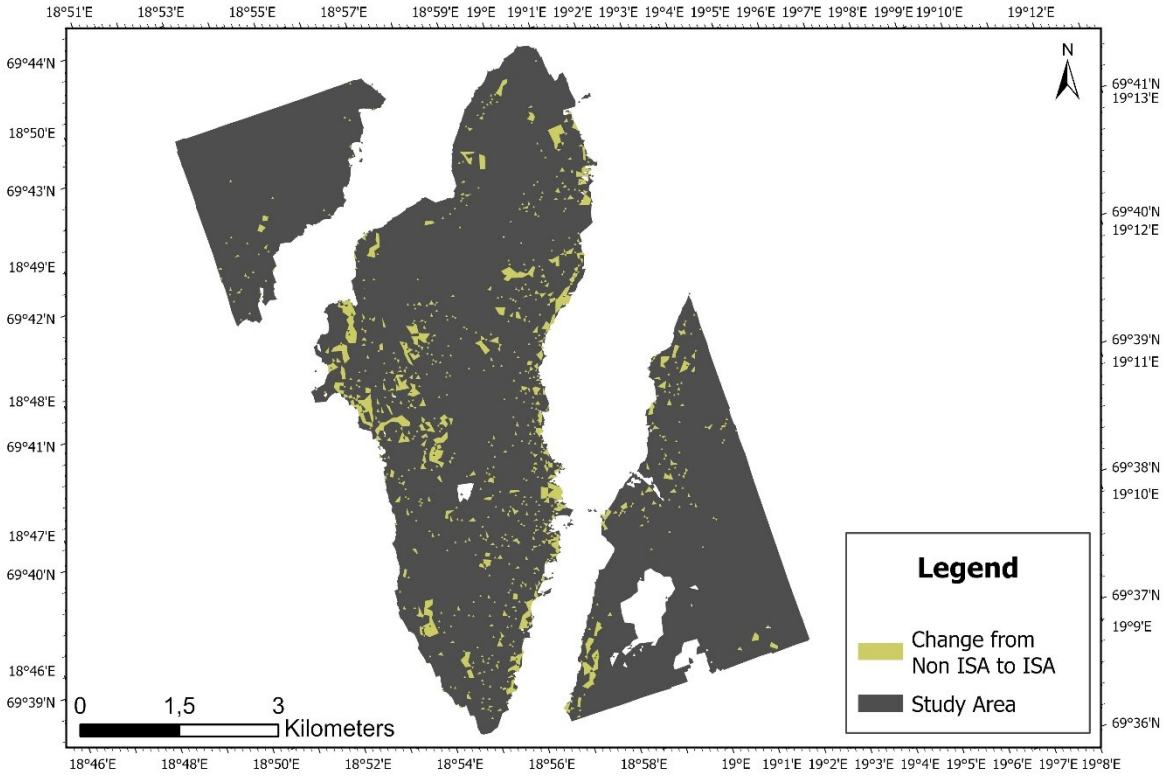

Figure 3.5. Change detection results, for 1993-2007 period

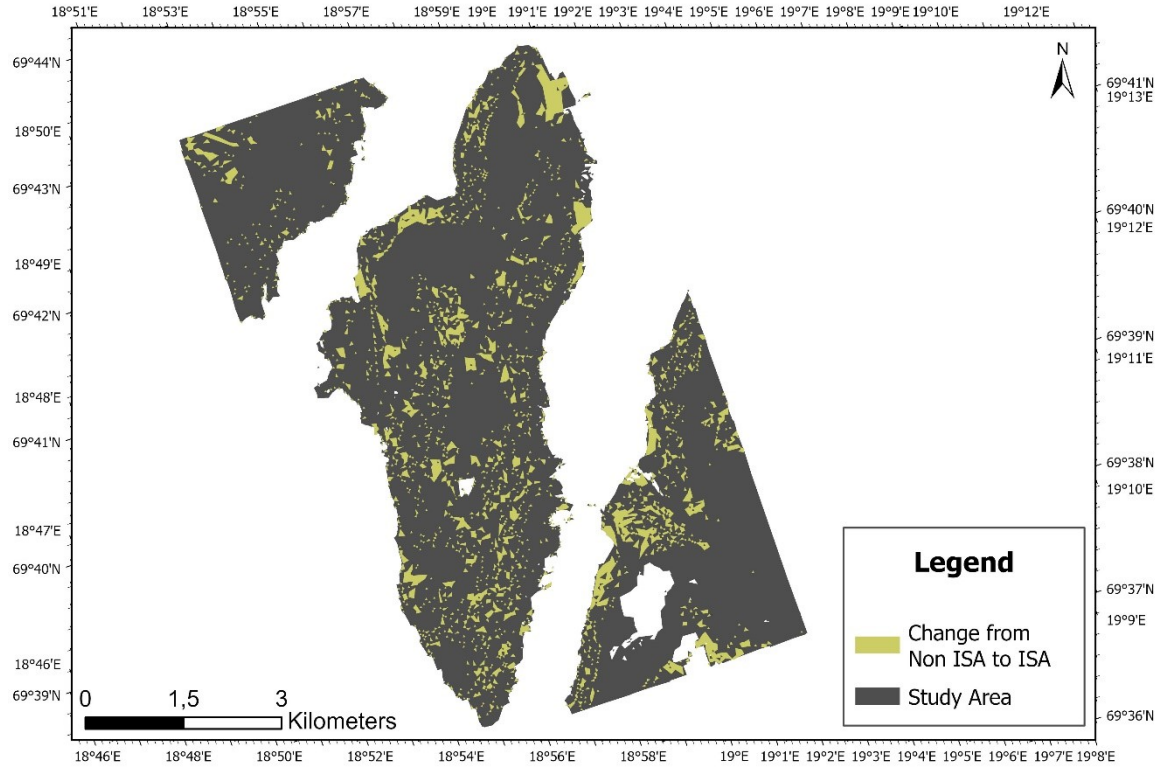

Figure 3.6. Change detection results, for 2007-2023 period

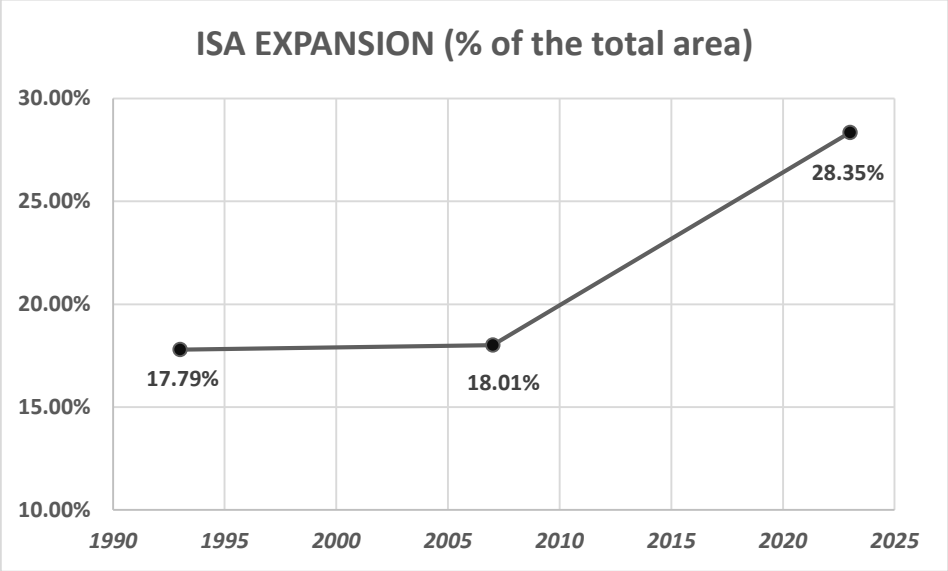

Figure 3.7. ISA expansion graph, based on SVM classification results.

As expected, the highest ISA growth is recorded in 1993-2023 period. ISA growth is detected across the whole study area, with a characteristic spread in the eastern part and in the island area of Tromso. From these changes, some limited are observed in 1993-2007 period, which are concentrated in the western and southwestern part of the island, as mentioned also in classification results. The majority of the detected changes are noticed in the 2007-2023 period, where the expansion of ISA throughout the whole island and also the eastern part of the study area, is highly marked.

4. DISCUSSION

This study implemented SVM classifier with medium spatial resolution imagery from Landsat and 9 to map ISA and detected changes from 1993 to 2023 in Tromso area, Norway. This method, in contrast to the traditional classification and change detection methods, provides a semi supervised tool for extracting ISA from Landsat data series, detecting alterations in the imperviousness of the surface, and calculating the changed areas simply by selecting the appropriate images and providing the training samples. SVM classifier is one of the most efficient and commonly used for land cover mapping, as shown by many studies (Cheng et al., 2011; Wei and Blaschke, 2018; Shao et al., 2023). In terms of classifier efficiency, the higher overall accuracy achieved can be attributed to SVM's ability to optimally delineating hyperplanes between classes when compared to alternative pixel-based techniques (Petropoulos et al., 2012). Unlike some methods that may not easily identify such hyperplanes, SVM has the ability to optimally generalize the separating hyperplane to unseen samples with minimum errors among various separating hyperplanes. This capability allows SVM to yield the most effective class separation in the final classification phase (e.g., Huang et al., 2002). It is also suitable for ISA monitoring, as SVM was originally developed as a binary linear classifier (Shi and Yang, 2015). This is also confirmed in the present study, where the performance of the classifier is accurately high. SVM yielded highly satisfactory results for the implemented study area, as indicated by the statistical metrics that were calculated. The findings presented in this study are like

those observed in other research endeavors that used the SVM technique with multispectral images in remote sensing applications (Wang et al., 2018; Liu et al., 2023; Zheng et al., 2023).

Various factors may be identified as potential sources of error in the technical execution of our case study, influencing the performance of the technique. On the one hand in all images, a notable removal of pixels has occurred due to the presence of clouds and cloud shadows. These removed pixels could potentially differentiate the quantitative results of the classification. On the other hand, several studies have demonstrated that there is a strong confusion in the spectral characteristics between impervious surfaces and bare soil (Su et al., 2022; Deng et al., 2020). Therefore, it is possible that pixels may have been incorrectly classified as ISA when representing bare ground.

At this point it is pertinent to refer to the correlation between ISAs and the demographic composition of the region. As can be derived from the data presented in Figure 4.1 the population dynamics of Tromso manifest a continuous upward trajectory from 1990 through 2020, a trajectory that extends through the year 2022. This substantiates the pivotal role played by ISAs in urban ecosystems, as the escalating extent of these surfaces (Figure 3.7) correlates with the concurrent demographic expansion within the purview of the study area.

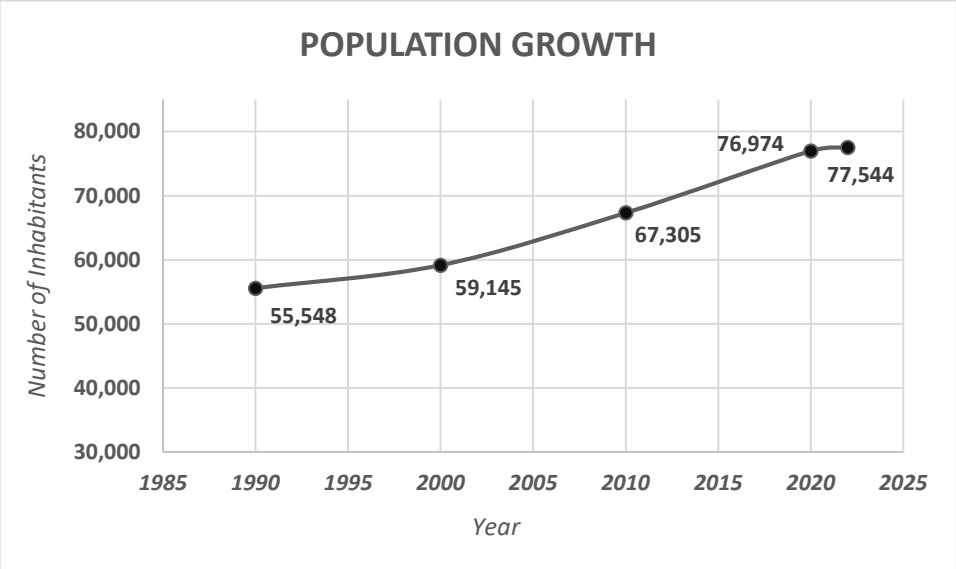

Figure 4.1. Population growth graph, from 1990 to 2022 (data obtained from Statistics Norway https://www.ssb.no/en)

This congruence underscores the complex interplay between anthropogenic infrastructure development, symbolized by the proliferation of ISAs, and the demographic dynamics shaping the urban landscape over the specified temporal span. This conclusion aligns with findings from related studies exploring the relationship between urban expansion and demographic trends (Melchiorri et al., 2018).

It is well known that the built-up area of cities cannot be accurately measured based on administrative boundaries. The analysis of remote sensing images makes it possible to delineate the total land area, the green areas (pervious surface) and the built-up areas (impervious surface). However, more sophisticated measurements are required when it comes to measuring urban built-up density, which includes the entire building area (DiNapoli and Jull 2020). Furthermore, urban expansion is not linear, as it takes very different forms in each city. It can take place through the

redevelopment of built-up areas at much higher densities, by filling in the remaining 'gaps' in already built-up areas or through the urban development of areas that were previously not used for urban purposes. New urban development can be adjacent to already built-up areas, or it can “leapfrog" outside built-up areas and create new urban space. In turn, it can reduce, maintain or increase open space in and around the city (Angel et al., 2005). Depending on the city, demographic expansion is linked to the urban landscape, but not exclusively to the consolidation of built-up areas, as a larger middle class tends to move to the urban fringe, triggering the formation of metropolitan regions or larger urban regions (Mahtta et al., 2022).

Another point worth mentioning is the performance of the Google Earth Engine (GEE) platform in the present study. Through GEE, a semi-automated methodology for the processing and analysis of Landsat images, coupled with their classification utilizing the machine learning SVM algorithm, was developed. The entire procedure was carried out in a cloud environment ensuring fast execution, with only the resultant outcomes being downloaded for subsequent visualization within the ArcGIS Pro software. The unique capabilities of GEE and other similar cloud-based platforms pave the way for new opportunities in ISA mapping in large geographical scales.

5. CONCLUSIONS

The Landsat images proved to be satisfactory for the specific application, as they are freely available and already pre-processed. Despite their medium resolution, they achieved high accuracy rates, justifying the widespread use of the SVM classifier in land cover mapping applications, specifically for ISA. The classification results can be considered successful, with very high accuracy rates of 93.18%, 95.13%, and 90.19% for each date, respectively. The kappa coefficient values are also highly satisfactory, ranging above 0.8 for all dates, confirming the agreement between classification results and ground truth values.

The outcomes of the classifications reveal a notable escalation in ISA, notably conspicuous within the 2007-2023 period, trend consistently corroborated by the findings of the change detection analyses. It is noteworthy that an initial correlation was made between these results, showing an increase in ISAs with the population evolution of the study area over time, observing a trend of consistency between the two variables.

Regarding the limitations of the study, they are confined to the absence of cloud-free images, resulting in the loss of portions of the study area due to cloud masking. Additionally, the confusion of pixel values between ISAs and bare soils poses challenges, as indicated in the literature.

The implementation of the whole methodology in GEE cloud platform represents a significant advancement in innovation. GEE is a robust platform for managing large-scale geospatial datasets, enabling seamless integration and analysis of Landsat imagery over extensive temporal and spatial scales. By harnessing GEE's cloud-based infrastructure, the computational load associated with processing Landsat time series data for ISA mapping is significantly reduced, fostering efficient analysis and prompt results. The combination of Landsat's multispectral data with the robust capabilities of the SVM classifier within the GEE framework enhances the accuracy and automation of ISA extraction while also facilitates change detection analyses by providing an extensive archive of Landsat images and proper algorithms for its calculation. This holistic approach, combining GEE, Landsat data and SVM classifier, proves pivotal in generating reliable and up-to-date information crucial for urban planning, environmental monitoring, and the study of climate change impacts.

In conclusion, the results of this study constitute a significant contribution to urban planning applications adapted to the socio-human factor. Also, the employed methodology has also the potential to be used operationally for real time monitoring of ISA while can be adaptive for application in diverse study areas, requiring adjustments only in the input parameters for the classification process. It can also be applicable to all dataset types available in GEE platform constituting a useful tool of analyzing urban environments. It can play a significant role in decision making in domes such as urban planning, policy making or natural hazards management.

ACKNOWLEDGMENTS

In the present research study, participation of all the co-authors, has been financially supported by the project "EO-PERSIST" European Union's Horizon Europe Research and Innovation program HORIZON-MSCA-2021-SE-01-01 under grant agreement N. 101086386.

REFERENCES

Adugna, T., Xu, W., & Fan, J. (2022). *Comparison of Random Forest and Support Vector Machine Classifiers for Regional Land Cover Mapping Using Coarse Resolution FY-3C Images*. Remote Sensing. https://doi.org/10.3390/rs14030574

Angel, S., Chabaeva, A., Gitlin, L., Kraley, A., Parent, J. & Perlin, M. (2005). The dynamics of global urban expansion. Washington, D.C.: World Bank Group. http://documents.worldbank.org/curated/en/138671468161635731/The-dynamics-of-global-urban-expansion

Cass, A., Petropoulos, G. P., Ferentinos, K. P., Pavlides, A., & Srivastava, P. K. (2019). Exploring the synergy between Landsat and ASAR towards improving thematic mapping accuracy of optical EO data. *Applied Geomatics*, *11*(3), 277–288. https://doi.org/10.1007/s12518-019-00258-7

Dawson, R. A., Petropoulos, G. P., Toulios, L., & Srivastava, P. K. (2019). *Mapping and monitoring of the land use/cover changes in the wider area of Itanos, Crete, using very high resolution EO imagery with specific interest in archaeological sites*. Environment, Development and Sustainability. https://doi.org/10.1007/s10668-019-00353-0

De Melo Cartaxo & Johana M Castilla & Marcin Dymet & Kamrul Hossain, T. (2021). *Digitalization and smartening sustainable city development: an investigation from the high north European cities*. ideas.repec.org. https://ideas.repec.org/a/pop/journl/v5y2021i1p83-101.html

Deng, C., & Zhu, Z. (2020). *Continuous subpixel monitoring of urban impervious surface using Landsat time series*. Remote Sensing of Environment. https://doi.org/10.1016/j.rse.2018.10.011

DiNapoli, B., & Jull, M. (2020, December 1). Urban planning sustainability metrics for Arctic cities. *Environmental Research Letters*, *15*(12), 124023. https://doi.org/10.1088/1748-9326/abc37b

Estimation of impervious surface based on integrated analysis of classification and regression by using SVM. (2011, July 1). IEEE Conference Publication | IEEE Xplore. https://ieeexplore.ieee.org/abstract/document/6049864?casa_token=gSzXvQqwR3IAAAAA:e_eAVuTxHgu4rYsMqLPqmTB7RmHpMqKpCQbLQUtVm5_7YmAUZQr2QUkK4BVTDc-j1uprXpb4

Fang, H., Wei, Y., & Dai, Q. (2019, June 28). A Novel Remote Sensing Index for Extracting Impervious Surface Distribution from Landsat 8 OLI Imagery. *Applied Sciences*, *9*(13), 2631. https://doi.org/10.3390/app9132631

Fragou, S., Kalogeropoulos, K., Stathopoulos, N., Louka, P., Srivastava, P. K., Karpouzas, S., Kalivas, D., & Petropoulos, G. P. (2020). *Quantifying Land Cover Changes in a Mediterranean Environment Using Landsat TM and Support Vector Machines*. Forests. https://doi.org/10.3390/f11070750

Furberg, D., Ban, Y., & Nascetti, A. (2019, October 17). *Monitoring of Urbanization and Analysis of Environmental Impact in Stockholm with Sentinel-2A and SPOT-5 Multispectral Data*. Remote Sensing. https://doi.org/10.3390/rs11202408

Gong, P., Li, X., & Zhang, W. (2019, June). 40-Year (1978–2017) human settlement changes in China reflected by impervious surfaces from satellite remote sensing. *Science Bulletin*, *64*(11), 756–763. https://doi.org/10.1016/j.scib.2019.04.024

Häme, T., Sirro, L., Kilpi, J., Seitsonen, L., Andersson, K., & Melkas, T. (2020, May 29). *A Hierarchical Clustering Method for Land Cover Change Detection and Identification*. Remote Sensing. https://doi.org/10.3390/rs12111751

Henning, M., Westlund, H., & Enflo, K. (2022, November 25). Urban–rural population changes and spatial inequalities in Sweden. *Regional Science Policy & Practice*, *15*(4), 878–892. https://doi.org/10.1111/rsp3.12602

Li, X., Zhou, Y., Zhu, Z., Liang, L., Yu, B., & Cao, W. (2018, October). Mapping annual urban dynamics (1985–2015) using time series of Landsat data. *Remote Sensing of Environment*, *216*, 674–683. https://doi.org/10.1016/j.rse.2018.07.030

Liu, Z., Yang, J., & Huang, X. (2023, December 1). *Landsat-derived impervious surface area expansion in the Arctic from 1985 to 2021*. Science of the Total Environment. https://doi.org/10.1016/j.scitotenv.2023.166966

Lu, D., & Weng, Q. (2009, March). Extraction of urban impervious surfaces from an IKONOS image. *International Journal of Remote Sensing*, *30*(5), 1297–1311. https://doi.org/10.1080/01431160802508985

Mahtta, R., Fragkias, M., Güneralp, B., Mahendra, A., Reba, M., Wentz, E.A., & Seto, K.C. (2022). Urban land expansion: the role of population and economic growth for 300+ cities. *npj Urban Sustain 2*(5) . https://doi.org/10.1038/s42949-022-00048-y

Melchiorri, M., Florczyk, A. J., Freire, S., Schiavina, M., Pesaresi, M., & Kemper, T. (2018, May 16). *Unveiling 25 Years of Planetary Urbanization with Remote Sensing: Perspectives from the Global Human Settlement Layer*. Remote Sensing. https://doi.org/10.3390/rs10050768

Morabito, M., Crisci, A., Guerri, G., Messeri, A., Congedo, L., & Munafò, M. (2021, January 1). *Surface urban heat islands in Italian metropolitan cities: Tree cover and impervious surface influences*. Science of the Total Environment. https://doi.org/10.1016/j.scitotenv.2020.142334

Omurakunova, G., Bao, A., Xu, W., Duulatov, E., Jiang, L., Cai, P., Abdullaev, F., Nzabarinda, V., Durdiev, K., & Baiseitova, M. (2020, January 5). Expansion of Impervious Surfaces and Their Driving Forces in Highly Urbanized Cities in Kyrgyzstan. *International Journal of Environmental Research and Public Health*, *17*(1), 362. https://doi.org/10.3390/ijerph17010362

Pandey, P. C., Koutsias, N., Petropoulos, G. P., Srivastava, P. K., & Ben Dor, E. (2019). Land use/land cover in view of earth observation: data sources, input dimensions, and classifiers—a review of the state of the art. *Geocarto International*, *36*(9), 957–988. https://doi.org/10.1080/10106049.2019.1629647

Petropoulos, G. P., Arvanitis, K. G., & Sigrimis, N. (2012a). *Hyperion hyperspectral imagery analysis combined with machine learning classifiers for land use/cover mapping*. Expert Systems With Applications. https://doi.org/10.1016/j.eswa.2011.09.083

Petropoulos, G. P., Kalaitzidis, C., & Vadrevu, K. P. (2012c). *Support vector machines and object-based classification for obtaining land-use/cover cartography from Hyperion hyperspectral imagery*. Computers & Geosciences. https://doi.org/10.1016/j.cageo.2011.08.019

Petropoulos, G. P., Kontoes, C., & Keramitsoglou, I. (2012b). *Land cover mapping with emphasis to burnt area delineation using co-orbital ALI and Landsat TM imagery*. International Journal of Applied Earth Observation and Geoinformation. https://doi.org/10.1016/j.jag.2012.02.004

Petropoulos, G. P., Vadrevu, K. P., & Kalaitzidis, C. (2013). Spectral angle mapper and object-based classification combined with hyperspectral remote sensing imagery for obtaining land use/cover mapping in a Mediterranean region. *Geocarto International*, *28*(2), 114–129. https://doi.org/10.1080/10106049.2012.668950

Phan, T. N., & Kappas, M. (2017). *Comparison of Random Forest, k-Nearest Neighbor, and Support Vector Machine Classifiers for Land Cover Classification Using Sentinel-2 Imagery*. Sensors. https://doi.org/10.3390/s18010018

Popa ,A.M., Onose ,D.A., Sandric ,I.C., Dosiadis ,E.A., Petropoulos ,G.P., Gavrilidis ,A.A., Faka ,A. (2022). *Using GEOBIA and Vegetation Indices to Assess Small Urban Green Areas in Two Climatic Regions.* Remote Sensing., 14(19), pp. 4888. https://doi.org/10.3390/rs14194888

Santamouris, M. (2020, January 1). *Recent progress on urban overheating and heat island research. Integrated assessment of the energy, environmental, vulnerability and health impact. Synergies with the global climate change*. Energy and Buildings. https://doi.org/10.1016/j.enbuild.2019.109482

Shao, Z., Cheng, T., Fu, H., Li, D., & Huang, X. (2023, May 14). *Emerging Issues in Mapping Urban Impervious Surfaces Using High-Resolution Remote Sensing Images*. Remote Sensing. https://doi.org/10.3390/rs15102562

Shi, D., & Yang, X. (2015, January 1). *Support Vector Machines for Land Cover Mapping from Remote Sensor Imagery*. Springer Remote Sensing/Photogrammetry. https://doi.org/10.1007/978-94-017-9813-6_13

Shih, H. C., Stow, D. A., Tsai, Y. M., & Roberts, D. A. (2020, March). Estimating the starting time and identifying the type of urbanization based on dense time series of landsat-derived Vegetation-Impervious-Soil (V-I-S) maps – A case study of North Taiwan from 1990 to 2015. *International Journal*

of Applied Earth Observation and Geoinformation, *85*, 101987. https://doi.org/10.1016/j.jag.2019.101987

Su, S., Tian, J., Dong, X., Tian, Q., Wang, N., & Xi, Y. (2022, July 14). An Impervious Surface Spectral Index on Multispectral Imagery Using Visible and Near-Infrared Bands. *Remote Sensing*, *14*(14), 3391. https://doi.org/10.3390/rs14143391

Törmä, M., Härmä, P., Hatunen, S., Teiniranta, R., Kallio, M., & Järvenpää, E. (2011, October 6). Change detection for Finnish CORINE land cover classification. *SPIE Proceedings*. https://doi.org/10.1117/12.898069

Vivekananda, G., Swathi, R., & Sujith, A. (2020, June 4). Multi-temporal image analysis for LULC classification and change detection. *European Journal of Remote Sensing*, *54*(sup2), 189–199. https://doi.org/10.1080/22797254.2020.1771215

Wahap, N., & Shafri, H. Z. (2020, July 1). Utilization of Google Earth Engine (GEE) for land cover monitoring over Klang Valley, Malaysia. *IOP Conference Series: Earth and Environmental Science*, *540*(1), 012003. https://doi.org/10.1088/1755-1315/540/1/012003

Wang, S., Ma, Q., Ding, H., & Huang, L. (2018, January 1). *Detection of urban expansion and land surface temperature change using multi-temporal landsat images*. Resources, Conservation and Recycling. https://doi.org/10.1016/j.resconrec.2016.05.011

Whyte, A., Ferentinos, K., & Petropoulos, G. P. (2018). *A new synergistic approach for monitoring wetlands using Sentinels -1 and 2 data with object-based machine learning algorithms*. Environmental Modelling and Software. https://doi.org/10.1016/j.envsoft.2018.01.023

Wu, W., Li, C., Liu, M., Hu, Y., & Xiu, C. (2020, December 16). Change of impervious surface area and its impacts on urban landscape: an example of Shenyang between 2010 and 2017. *Ecosystem Health and Sustainability*, *6*(1). https://doi.org/10.1080/20964129.2020.1767511

Zhao, Y., & Zhu, Z. (2022, March). ASI: An artificial surface Index for Landsat 8 imagery. *International Journal of Applied Earth Observation and Geoinformation*, *107*, 102703. https://doi.org/10.1016/j.jag.2022.102703

Zheng, Z., Yang, B., Liu, S., Xia, J., & Zhang, X. (2023, April 1). *Extraction of impervious surface with Landsat based on machine learning in Chengdu urban, China*. Remote Sensing Applications: Society and Environment. https://doi.org/10.1016/j.rsase.2023.100974